LAWRENCE
LIVERMORE
NATIONAL
LABORATORY

LLNL-JRNL-411044

Aspect Ratio Effects in the Driven, Flux-Core Spheromak

E. B. Hooper, C. A. Romero-Talamás, L. L. LoDestro, R. D. Wood, H. S. McLean

March 4, 2009

Physics of Plasmas

Disclaimer

Aspect ratio effects in the driven, flux-core spheromak

E. B. Hooper,[a] C. A. Romero-Talamás,[b] L. L. LoDestro, R. D. Wood, and H. S. McLean
Lawrence Livermore National Laboratory
P. O. Box 808
Livermore, CA 94551

Resistive magneto-hydrodynamic simulations are used to evaluate the effects of the aspect ratio, A (length to radius ratio) in a spheromak driven by coaxial helicity injection. The simulations are benchmarked against the Sustained Spheromak Physics Experiment (SSPX) [R. D. Wood, et al., Nucl. Nucl. Fusion **45**, 1582 (2005)]. Amplification of the bias ("gun") poloidal flux is fit well by a linear dependence (insensitive to A) on the ratio of gun current and bias flux above a threshold dependent on A. For low flux amplifications in the simulations the n=1 mode is coherent and the mean-field geometry looks like a tilted spheromak. Because the mode has relatively large amplitude the field lines are open everywhere, allowing helicity penetration. Strongly-driven helicity injection at $A \leq 1.4$ in simulations generates reconnection events which open the magnetic field lines; this state is characteristic of SSPX. Near the spheromak tilt-mode limit, $A \approx 1.67$ for a cylindrical flux conserver, the tilt approaches 90°; reconnection events are not generated up to the strongest drives simulated. The time-sequence of these events suggests that they are representative of a chaotic process. Implications for spheromak experiments are discussed.

PACS: 52.55.Ip, 52.65.Kj

[a]Electronic email: hooper1@llnl.gov
[b]Present address: IREAP, University of Maryland, College Park, MD 20742-3511.

I. Introduction

The spheromak[1] is a toroidal, magnetic confinement configuration usually formed in a singly-connected volume, with no central post and thus no toroidal magnetic field coil or transformer to drive current. The current and magnetic field are generated by injecting linked toroidal and poloidal magnetic fluxes (and thus magnetic helicity) into a flux-conserving vessel. A magnetic dynamo reconfigures these fluxes at constant helicity into the spheromak configuration. In experiments such as Beta II,[2] the Compact Torus Experiment (CTX),[3] the Flux Amplification Compact Torus (FACT),[4] SPHEX[5] and the Sustained Spheromak Physics Experiment (SSPX),[6] helicity is injected by a coaxial plasma gun and sometimes called coaxial helicity injection (CHI);[7] the resulting magnetic configuration is a flux-core spheromak.

Helicity injection can be used to form and buildup the spheromak as well as to sustain it. The magnitudes of the generated spheromak poloidal flux and toroidal plasma current need to be high as do the efficiencies of generating and sustaining them. Generally, however, the achieved, experimental values are considerably less than desired for a high magnetic field, fusion plasma.[8] In this paper we use resistive MHD simulations, benchmarked against experiment, to examine the role of the spheromak aspect ratio, A (length divided by radius) on these quantities and the physics of their generation. The issue of obtaining high temperatures and good energy confinement[6] once the spheromak is formed will not be addressed here.

In CHI, the injected poloidal flux is provided by an applied (bias) poloidal flux, ψ_g, between the gun and flux conserver, and the injected toroidal flux is generated by the gun current, I_g, so that the rate of helicity injection into the flux conserver is $\dot{K} = 2V_g\psi_g$ where V_g is the voltage across the insulating gap.[9] In SSPX experiments, magnetic reconnection events then reconfigure the injected fluxes into the spheromak geometry.[10] The net result of this dynamo is to generate a poloidal flux difference, ψ_0, between the spheromak magnetic axis and the geometric axis at a flux amplification factor $F_a = \psi_0/\psi_g$ greater than the bias (gun) flux. The value of F_a is an important measure of the effectiveness of the helicity

injection; a large value is needed to generate the high poloidal fluxes needed for good plasma confinement, but it also determines the power losses on the open magnetic field lines relative to those inside the separatrix.[8] This is because the poloidal flux in the open (edge) field lines equals the applied bias in a strongly-driven, flux-core spheromak; thus the area of the edge plasma relative to the closed plasma scales essentially as ψ_g/ψ_0. Ohmic losses on the open edge field lines are high because the electron temperature there is low, and it is estimated that $F_a \approx 50$ is required for the losses to be acceptable for a spheromak fusion reactor.[11]

Among the factors that can influence the flux amplification is the geometry of the flux conserver. Most experiments have been conducted in approximately cylindrical flux conservers with the length to radius ratio, $L_{fc}/R_{fc} \sim 1$, albeit with different helicity injector ("gun") geometries. An aspect ratio of 1 provides a substantial margin of safety against the tilt mode,[12] which is known to occur in spheromaks which are isolated from the gun when $L_{fc}/R_{fc} \approx 1.67$.[13, 14] It is difficult to change the flux conserver, especially in a high-powered experiment with well conditioned walls, so varying L_{fc}/R_{fc} in experiments is rare and has not been done systematically. CTX made a number of changes of this ratio,[15] but they were small, and the dimensions of the gun entrance region were often changed simultaneously as was the high-voltage power supply configuration, so no scaling was deduced for the effects of the flux conserver geometry.[1] SSPX made one change in the flux-conserver length[16] which will be used to benchmark the simulations discussed below.

Single fluid, resistive MHD simulations of spheromaks using the NIMROD code[17] have been quite successful in describing the behavior of SSPX[18] with flux amplification especially well predicted,[6, 8] so simulations can be used with some confidence to explore the effects of the aspect ratio. In Section II we consider simulations in the SSPX geometry, varying L_{fc} and determining F_a. Confidence in the results is strengthened by comparisons with experimental data where possible. As will be seen, there will be a reduction in the threshold value of $\lambda_g = \mu_0 I_g/\psi_g$ for forming the spheromak as the aspect ratio increases, but $dF_a/d\lambda_g$ is almost constant.

A variety of fluctuation dynamics (four "Classes") ranging from low-amplitude, $n = 1$ modes to nonsteady, relaxation events were observed in flux-core spheromak simulations done by Sovinec, et al.[17] primarily in a pillbox geometry. The MHD equations used in the present simulations are extended from those in Ref. 17 by including temperature evolution in the presence of anisotropic thermal conductivity; see Ref. 18 for details. Similar dynamics are seen herein at fixed gun current as in the previous simulations at fixed gun voltage, although we also find that the pinched gun-current column can be unstable to a steady-state n=1 mode below the threshold for flux amplification. At low flux amplification the $n = 1$ mode becomes steady after the amplification saturates, as in Sovinec, et al. (This behavior was not observed in the SSPX experiment, although low flux-amplification spheromaks were not studied extensively.) At high amplification a nonsteady state occurs, although the nonsteady behavior is chaotic in time at the highest amplifications, extending this Class beyond that reported for the earlier simulations. Section III will therefore consider the characteristics of the sustainment of SSPX when strongly driven, including the dynamo associated with relaxation events in which magnetic reconnection results in open magnetic field lines, rearrangement of the fluxes into the spheromak geometry, and gun voltage spikes from the resulting change in the power-supply load inductance.[10] The time history of these events in SSPX simulations (in this regime) and experiment is consistent with a nearly chaotic system.

We will find in Section IV that the nature of the dynamo changes as the geometry approaches L_{fc}/R_{fc} ~1.67. At the higher aspect ratio, the dynamo is a large amplitude, toroidal mode number $n = 1$ mode at nearly constant amplitude, and the mean-field spheromak is highly tilted. Because of the large plasma asymmetry, magnetic field lines are stochastic throughout most of the axisymmetric flux conserver, allowing helicity and current to penetrate the spheromak. When the spheromak is quite strongly driven, the simulation has problems converging and may be evolving towards an almost fully tilted geometry. Relaxation events are not found in any of the simulations conducted in this geometry.

The paper will finish with a discussion exploring whether this behavior can explain some of the differences among spheromak experiments, followed by conclusions and recommendations for further work.

II. Flux amplification and spheromak aspect ratio

A detailed comparison of the measured flux amplification in SSPX with the predictions of a resistive MHD simulation using the NIMROD code found excellent agreement near the threshold.[8, 6] For completeness, the comparison is reproduced in Fig. 1a. The saturation onsetting at $\lambda_g > 13$ m^{-1} in the experiment was not seen in the simulations. In an experimental run in SSPX near the end of its operation the aspect ratio was increased to 1.2;[16] measurements are compared with simulations in Fig. 1b. The agreement is good, although less so than seen in Fig. 1a, perhaps due to relatively poor vacuum conditions; the increased flux-conserver length was obtained by lengthening the diagnostic access slot at the spheromak midplane, and the plasma sputtered considerable copper from the vertical bars carrying wall current across the gap. In support of this hypothesis, the plasma quality was observed to decrease throughout the run, and data from early in the run had the best agreement with simulations.

For both aspect ratios, the flux amplification was well fit above a threshold by

$$F_a = 1 + \alpha\left(\lambda_{gun} - \lambda_{th}\right) \tag{1}$$

For L_{fc}/R_{fc} =1, $\lambda_{th} = 10.0$ m^{-1} and for $L_{fc}/R_{fc} = 1.2$, $\lambda_{th} = 7.5$ m^{-1}; in both cases, $\alpha =$ 0.56 m. Perhaps coincidentally, the flux-conserver radius is 0.5 m.

Simulations were also run for $L_{fc}/R_{fc} = 1.4$ and 1.6; see Figs. 1c and 1d. Linear fits as in Eq. (1) were also found, although with slightly larger values of α. Note that F_a is found from the $n = 0$ component of the magnetic field. Later in this paper we will see that the spheromak axis is tilted from the vertical, especially when A is near the tilt-mode limit for the flux conserver. In this case the axisymmetric component of the field is insufficient to fully describe the built-up state.

The fits are summarized in Table 1. Also shown is the lowest eigenvalue of the flux conserver, estimated from $\nabla \times \mathbf{B} = \lambda_{FC}\mathbf{B}$ in the cylindrical approximation, $\lambda_{FC} = \sqrt{\left(3.83/R_{fc}\right)^2 + \left(\pi/L_{fc}\right)^2}$, which is > λ_{th} except at $A = 1$. Both experimental reconstructions and simulations find that the current peaks strongly along the geometric axis for long (millisecond) discharges, so that the value of $\lambda = \mu_0 \mathbf{j}\cdot\mathbf{B}/B^2$ on that axis exceeds λ_{FC}, while the value on the separatrix is less. An example from experiment is shown in Fig. 2a, and one from simulation is shown in Fig. 2b. In both cases, λ on the separatrix is well below λ_{FC}. These profiles thus satisfy the condition that the $\lambda(r)$ profile must span λ_{FC}.[19] This radial variation makes simple approximations, for example assuming constant λ in the edge plasma, inadequate for predicting the flux amplification.

III. Dynamo characteristics in a strongly-driven spheromak at $A = 1$..

In many spheromak experiments, the buildup and sustainment of the magnetic field during the formation with $\lambda_g > \lambda_{th}$ is accompanied by spikes on the electrode voltage. An example from SSPX is shown in Fig. 3. Spikes are also seen in resistive MHD simulations where they are identified as resulting from magnetic reconnection events.[10] An example of this behavior from a simulation is shown in Fig. 4 which illustrates an approximately 100 μs history of a strongly-driven spheromak.

The behavior between the second and third voltage spikes in Fig. 4 is expanded in Figs. 5 and 6. At each spike the temperature, T, and the energy in the $n = 1$ mode both drop rapidly. Magnetic field lines become stochastic throughout the flux-conserver volume, allowing current and flux to penetrate from the edge plasma and heat to flow along field lines to the wall. Following this, flux surfaces heal in the spheromak core while the energy in the $n = 1$ mode increases until the voltage spikes again. Behavior very much like this was found using magnetic probes in the FACT spheromak.[4]

Three-dimensional visualizations during this simulation using the software system VISIT[20] are shown in Fig. 7. In these plots the constant-λ surface has been chosen to represent the current column along the geometric axis and the

constant-T surface has been chosen as a proxy for the flux surfaces which often exist only in a mean-field (approximate) sense.

The constant-T surfaces can take rather more complex shapes than seen in Fig. 7; c.f. Fig. 8. Contour plots for the temperature in Fig. 9 often show stellarator-like surfaces with the $n = 1$, $m = 1$ shape corresponding to the dominant mode in the plasma even though magnetic surfaces are not closed. A magnetic field puncture plot for this time is shown in Fig. 10. The field line shown is stochastic, but confined between two Kolmogorov-Arnold-Moser (KAM, see, e.g. Ref. 21) surfaces and followed for $> 10^3$ m in our study. The lowest Liapunov exponent for this field line, characteristic of the mean exponential rate of divergence of nearby field lines, was calculated using the method of Benettin, et al.,[22] and corresponds to a length of 5.0 times around the torus toroidally. Consequently, field lines deviate from an initial, axisymmetric starting surface quite slowly and mean-field surfaces are well defined. Consistent with this conclusion, constant temperature contours in this region are helical (m=1, n=1) surfaces as seen in Fig. 9, even though there are no true, closed magnetic surfaces in this region. At other times, of course, the deviation of field lines from the initial surface is faster, although the geometry of the *mean* field is still quite close to that of the ideal spheromak. The field-line puncture plots shown in Figs. 6 and 10 show that the magnetic field is often stochastic and can be ergotic in the sense that a line can visit the entire volume.

For the SSPX experiment the generation of stochastic field lines is seen to occur in a relaxation oscillator-like behavior which itself appears to be chaotic in time. This is meant in the sense that the chaos is characteristic of the full dissipative system rather than just stochastic field lines which can be described by a Hamiltonian. The cathode-voltage autocorrelation function provides a simple, first test of this hypothesis. Thus, for both experimental data and numerical data from the resistive MHD simulations, the autocorrelation function was calculated as:

$$C(\tau) = \frac{1}{i_m} \sum_{i=i_0}^{i_0+i_m} \left(V_i - \overline{V}\right)\left(V_{i+i_n} - \overline{V}\right) \qquad (1)$$

with $\tau = i_n \Delta t$ and Δt the time between the voltage samples; i_m is the sample length and is many voltage pulses long. Figure 11 compares the autocorrelation function for a SSPX discharge (Fig. 3) and a simulation (Fig. 4).

The high peak at $\tau = 0$ is characteristic of a random process. The width of the experimental result is limited by the sample time of the data, 1 μs, but higher-speed measurements on other discharges indicated that the width of the voltage spikes was close to 1 μs. (Unfortunately, the amplitude resolution was inadequate to calculate the autocorrelation function.) Interestingly, both autocorrelation functions in Fig. 11 show a low-amplitude oscillation with a period of 6-7 μs. This does not appear to correspond to the average time between the spikes and has not been previously identified in the data.

Sovinec, et al.[17] identified a nonsteady state which was periodic (their Class four), and these are seen in some of our simulations. The low-amplitude oscillation in the autocorrelation function is likely the residual effect of this periodicity.

Thus, for $A \leq 1.4$ (Fig. 1), simulations at the lowest values of λ_g behave coherently, but at the highest drive the voltage behavior has become chaotic. Such transitions are a well-known characteristic of dissipative systems, consistent with considering the driven spheromak a system which can become chaotic; see, for example, the discussion in Ref. 21. As noted in this reference there are many "paths" to chaos; it is not clear which applies to the spheromak.

IV. Dynamo characteristics at an aspect ratio close to the tilt limit.

In spheromak simulations in a flux conserver very near the tilt limit the n=1 mode is coherent (approximately a sine wave) at flux amplifications up to > 3 and has a large amplitude, as seen for A= 1.6 in Fig. 12. A simulation at $\lambda_g = 11.9$ m^{-1}, however, found the flux amplification increasing steadily towards the fit shown in Fig. 1d when the mode amplitude increased abruptly and the $n = 0$ component of the flux decreased abruptly. It appears that the spheromak tilt increased significantly; numerical convergence became difficult and the simulation was discontinued.

At $\lambda_g < 11.9$ m^{-1}, the constant temperature surfaces (Fig. 13) are stellarator-like and strongly tilted; the field lines are chaotic throughout most of the volume. Near the magnetic axis some closed, stellarator-like surfaces exist as seen in Fig. 14. These surfaces are very similar to ones seen by Sovinec, et al.[17] and Finn, et al.[23] in a simulation of a strongly-driven spheromak, who observed that the non-axisymmetric configuration is driven by currents in the plasma outside these surfaces and that there is no helicity transport across them. We also observed them at low flux amplification in lower aspect ratio simulations.

In the elongated flux conserver, therefore, current and flux can penetrate into the spheromak although not into the stellarator-like regions. The $n = 0$ component of the magnetic field closely approximates the lowest eigenfunction of the flux conserver, but the plasma is highly tilted, and its axis precesses around the geometric axis. In the present simulations, this precession rate is affected by the boundary condition for the azimuthal velocity at the wall which has been chosen to approximate observations in SSPX which presumably are determined by processes outside resistive MHD.[17]

V. Discussion and conclusions

The simulations yield a simple, off-set linear relation between flux amplification and λ_g, with $dF_a/d\lambda_g$ only weakly dependent on the aspect ratio. The available experimental data from SSPX track this behavior until F_a starts to saturate, apparently for reasons that lie outside the single-fluid resistive MHD model. (The saturation seen in Ref. 17 was in a spheromak driven by voltage source, not the current source used here.) The characteristics of the nonlinear steady state behavior extend the four classes in Sovinec, et al. by including an oscillating, column-driven mode below the λ_g-threshold for flux amplification and a nearly-chaotic state in strongly driven spheromaks.

The transport of helicity into the core of the spheromak requires that magnetic field lines be open at least part of the time, as observed during steady-state, large-amplitude oscillations and during bursty reconnection events: Helicity transport across closed magnetic surfaces is absent in ideal MHD and is

of order the resistivity in resistive MHD.[24, 25, 26] Thus, the amplification of magnetic flux found in the SSPX simulations occurs when the field lines are stochastic: (1) For flux conservers far from the tilt-unstable aspect ratio, the system exhibits steady oscillations at low drive. and during strong drive, relaxation oscillations with voltage spiking when a reconnection event occurs. (2) For simulations of the flux conserver close to the tilt limit, there is a large, constant-amplitude column mode ($n = 1$); it is an open question whether a strongly-driven spheromak will behave chaotically.

These results may explain why some spheromaks behave in a different manner than SSPX. The SPHEX experiment,[5] in particular, typically showed a much more coherent behavior for the $n = 1$ mode[27] than SSPX or CTX. In its standard operation with a positively-biased gun, the column carrying the gun current had a structure typified as a steady, rotating "dough-hook," which looked much like the column shown in Fig. 13. Negative-gun operation was also relatively coherent, although the dough-hook effect was absent.[28] The SPHEX flux conserver had an aspect-ratio of unity but was nearly spherical in shape; a spherical flux conserver is marginally stable to the tilt mode[12] In addition, there was a rather large entrance channel between the gun and the flux conserver. This geometry was thus likely to be closer to the tilt limit than SSPX, allowing the large-amplitude, coherent behavior as observed herein at large aspect ratio. Simulations of SPHEX would be required to verify this conjecture.

As discussed in Ref. 16, the efficiency of spheromak formation, e.g. as given by B_p/I_g, with B_p the poloidal field measured at the wall, increases as the flux conserver is lengthened. This measure of efficiency is proportional to F_a/λ_g, and thus scales as $\alpha + (1 - \alpha\lambda_{th})/\lambda_g$. The increase in efficiency near threshold between the aspect ratio 1 and 1.6 flux conservers is seen to be 1.4 and at large λ_g is 1.2. These factors are not sufficient to reach the efficiencies needed for a fusion-quality plasma. Furthermore, the increased flux amplification is achieved by operating nearer the tilt instability, thereby increasing the strength of the symmetry-breaking, $n = 1$ mode.

This analysis is, of course, only one possible variation in the spheromak geometry. Other shape effects, such as the "bow-tie" flux conserver which is

predicted to have higher beta limits than the cylinder,[29] or as the placement and size of the gun, should be examined for buildup efficiency in future work or in designs for new spheromak experiments.

ACKNOWLEDGMENTS

We thank the SSPX experimental team for their extensive efforts during the operation of the experiments. Stimulating discussions with B. I. Cohen are gratefully acknowledged, as is C. R. Sovinec's help with the NIMROD code and spheromak physics in general. The visualization in this work was made possible by the help of Brian Nelson at the PSI Center, University of Washington, who prepared the python code scripts which converted the NIMROD output into the proper format for VISIT. Brad Whitlock of LLNL provided much-needed consulting guidance on the use of VISIT, and W. H. Meyer of LLNL installed and debugged the code on a local computer system and provided important support as needed. The simulations made use of resources at the National Energy Research Supercomputer Center under Department of Energy Contract No. DE-AC03-76SF00098. The work was performed under the auspices of the U. S. Department of Energy by Lawrence Livermore National Laboratory under contracts W7405-ENG-48 and DE-AC52-07NA27344.

Table 1. Flux-amplification parameters.

L_{fc}/R_{fc}	λ_{th}	α	λ_{FC}
1.0	10	0.56	9.9
1.2	7.5	0.56	9.3
1.4	6.9	0.625	8.9
1.6	7.1	0.68	8.6

References

[1]T. R. Jarboe, Plasma Phys. Control. Fusion **36**, 945 (1994).

[2]W. C. Turner, G. C. Goldenbaum, E. H. Granneman, J. H. Hammer, C. W. Hartman, D. S. Prono, and J. Taska, Phys. Fluids **26**, 1965 (1083).

[3]T. R. Jarboe, F. J. Wysocki, J. C. Fernández, I. Henins, and G. J. Marklin, Phys. Fluids B, 1342 (1990).

[4]M. Nagata, T. Kanki, T. Matsuda, S. Naito, H. Tatsumi, and T. Uyama, Phys. Rev. Letters **71**, 4342 (1995).

[5]M. G. Rusbridge, S. J. Gee, P. K. Browning, G. Cunningham, R. C. Duck, A. al-Karkhy, R. Martin, and J. W. Bradley, Plasma Phys. Control. Fusion **39**, 683 (1997).

[6]B. Hudson, R. D. Wood, H. S. McLean, E. B. Hooper, D. N. Hill, J. Jayakumar, J. Moller, D. Montez, C. A. Romero-Talamás, T. A. Casper, J. A. Johnson III, L. L. LoDestro, E. Mezonlin, and L. D. Pearlstein, Phys. Plasmas **15**, 056112 (2008).

[7]T. R. Jarboe, private communication.

[8]E. B. Hooper, D. N. Hill, H. S. McLean, C. A. Romero-Talamás, and R. D. Wood, Nucl. Fusion **47**, 1064 (2007).

[9]T. H. Jensen and M. S. Chu, Phys. Fluids **27**, 2881 (1994).

[10]E. B. Hooper, T. A. Kopriva, B. I. Cohen, D. N. Hill, H. S. McLean, R. D. Wood, and S. Woodruff, Phys. Plasmas **12**, 092503 (2005).

[11]R. L. Hagenson and R. A. Krakowski, Fusion Technology **8**, 1606 (1985).

[12]M. N. Rosenbluth and M. N. Bussac, Nucl. Fusion **19**, 489 (1979).

[13]J. M. Finn, W. M. Manheimer, and E. Ott, Phys. Fluids **24**, 1336 (1981).

[14]A. Bondeson, G. Marklin, Z. G. An, H. H. Chen, Y. C. Lee, and C. S. Liu, Phys. Fluids **24**, 1682 (1981).

[15]C. W. Barnes, T. R. Jarboe, G. J. Marklin, S. O. Knox, and I. Henins, Phys. Fluids B **2**, 1871 (1990).

[16]R. D. Wood, D. N. Hill, H. S. McLean, E. B. Hooper, B. F. Hudson, J. M. Moller, and C. A. Romero-Talamás, Nucl. Fusion **49**, 025001 (2009).

[17]C. R. Sovinec, J. M. Finn, and D. del-Castillo-Negrete, Phys. Plasmas **8**, 475 (2001).

[18]E. B. Hooper, B. I. Cohen, H. S. Mclean, R. D. Wood, C. A. Romero-Talamás, and C. R. Sovinec, Phys. Plasmas **15**, 032502 (2008).

[19]D. A. Kitson and P. K. Browning, Plasma Phys. Control. Fusion **14**, 1265 (1990).

[20]See http://www.llnl.gov/visit.

[21]R. C. Hilborn, *Chaos and Nonlinear Dynamics* (Oxford, New York, 2000), 2nd Edition, Chapter 4.

[22]G. L. Benettin, L. Galgani, and J. M. Strelcyn, Phys. Rev. **A14**, 2338 (1976).

[23]J. M. Finn, C. R. Sovinec, and Diego del-Castillo-Negrete, Phys. Rev. Letters **85**, 4538 (2000).

[24]A. H. Boozer, Phys. Fluids B **5**, 2271 (1993).

[25]R. W. Moses, R. A. Gerwin, and K. F. Schoenberg, Phys. Plasmas **8**, 4839 (2001).

[26]R. R. Mett and J. B. Taylor, Phys. Fluids B **4**, 73 (1991).

[27]R. C. Duck, P. K. Browning, G. Cunningham, S. J. Gee, A. al-Karkhy, R. Martin, and M. G. Rusbridge, Plasma Phys. Control. Fusion **39**, 715 (1997).

[28]S. Woodruff and M. Nagata, Plasma Phys. Control. Fusion **44**, 2539 (2002).

[29]T. R. Jarboe, F. J. Wysocki, J. C. Fernández, I. Henins, and G. J. Marklin, Phys. Fluids B **2**, 1342 (1990).

[30]See EPAPS Document No. .... For more information on EPAPS, see http://www.aip.org/pubservs/epaps.html.

Figure Captions

Fig. 1. (Color online) (a) Comparison of flux amplification in SSPX and in NIMROD simulations. These results are in the standard flux conserver with R = 0.5 m and L = 0.5 m. (b) Comparison of flux amplification in the SSPX extended flux conserver with NIMROD simulations. These results had R = 0.5m and L = 0.6 m. (c) Flux amplification from simulation for L_{fc}/R_{fc} = 1.4. (d) Flux amplification for L_{fc}/R_{fc} = 1.6; see the discussion in Sec. IV regarding a simulation at λ_g = 11.9 m^{-1}.

Fig. 2. (Color online) (a) Profile of λ from SSPX, found by fitting the solution to the Grad-Shafranov equation to magnetic probe measurements on the flux-conserver walls. (b) Contours of λ (axisymmetric part) from the simulation for L_{fc}/R_{fc} = 1.4 with λ_g = 7.7 m^{-1} and λ_{FC} = 8.9 m^{-1}. Constant poloidal flux is in gray with the separatrix (λ = 6.4 m^{-1}) in black. This example is for a flux amplification of 1.5.

Fig. 3. (Color online) Buildup of magnetic field in a discharge in SSPX illustrating voltage spiking when $\lambda_g > \lambda_{th}$.

Fig. 4. (Color online) Voltage, magnetic field energy, and temperature during a 100 μs history in a simulation.

Fig. 5. (Color online) Voltage, temperature, and magnetic energy evolution between two voltage spikes in Fig. 4.

Fig. 6. (Color online) Field line Poincaré ("puncture") plots at 4 different times in the simulation shown in Fig. 5, showing the breakup and healing of flux surfaces near the magnetic axis.

Fig. 7. (Color online) Surfaces of constant λ = 14 m^{-1} (blue column) and constant T = 95% of the peak value (red torus) at the times shown in Fig. 7. In this

simulation, $\lambda_g = 20.3\ m^{-1}$ A movie (newbank1A2.mpeg) showing the evolution of these surfaces is available in Ref. 30.

Fig. 8. (Color online) Constant λ and constant T surfaces as in Fig. 7, showing a more complex geometry.

Fig. 9. (Color online) Constant temperature surfaces in the poloidal plane at toroidal angles of 0, $\pi/2$, π, and $3\pi/2$.

Fig. 10. (Color online) A puncture plot for a single field line in Fig. 8b. The field line is confined to the volume shown for at least 1000m.

Fig. 11. (Color online) Autocorrelation function for: (a) an experimental discharge and (b) a simulation.

Fig. 12. (Color online) Top-to-bottom: Voltage, magnetic energy, and temperature for the elongated flux conserver, L/R=1.6.

Fig. 13. (Color online) Constant $\lambda = 9.5\ m^{-1}$ surface (blue column) and T surface at 85% of the peak value (red torus) for the elongated flux conserver. Here $\lambda_g = 10.5\ m^{-1}$. A movie (SSPX_longb2.mpeg) showing the evolution of these surfaces is available in Ref. 30.

Fig. 14. (Color online) Stellarator-like magnetic surfaces near the magnetic axis are imbedded in a stochastic sea of open field lines.

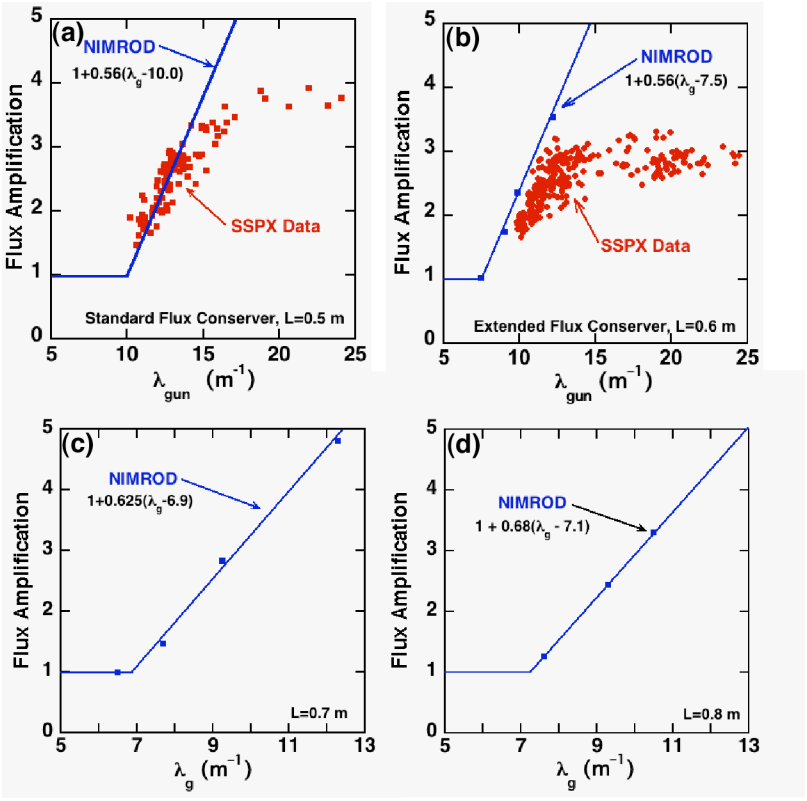
(a)
NIMROD
1+0.56(λg-10.0)
SSPX Data
Standard Flux Conserver, L=0.5 m
Flux Amplification
λgun (m-1)
(b)
NIMROD
1+0.56(λg-7.5)
SSPX Data
Extended Flux Conserver, L=0.6 m
Flux Amplification
λgun (m-1)
(c)
NIMROD
1+0.625(λg-6.9)
L=0.7 m
Flux Amplification
λg (m-1)
(d)
NIMROD
1 + 0.68(λg - 7.1)
L=0.8 m
Flux Amplification
λg (m-1)

Fig. 1

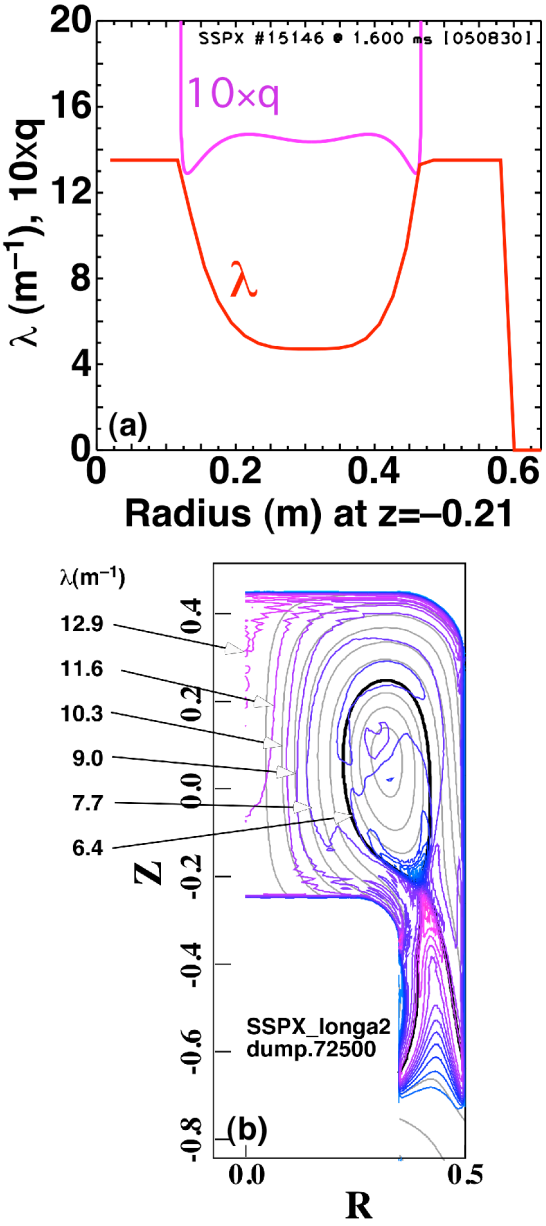
SSPX #15146 ● 1.600 ms [050830]
10×q
λ
λ (m⁻¹), 10×q
(a)
Radius (m) at z=–0.21
λ(m⁻¹)
12.9
11.6
10.3
9.0
7.7
6.4
Z
SSPX_longa2
dump.72500
(b)
R

Fig. 2.

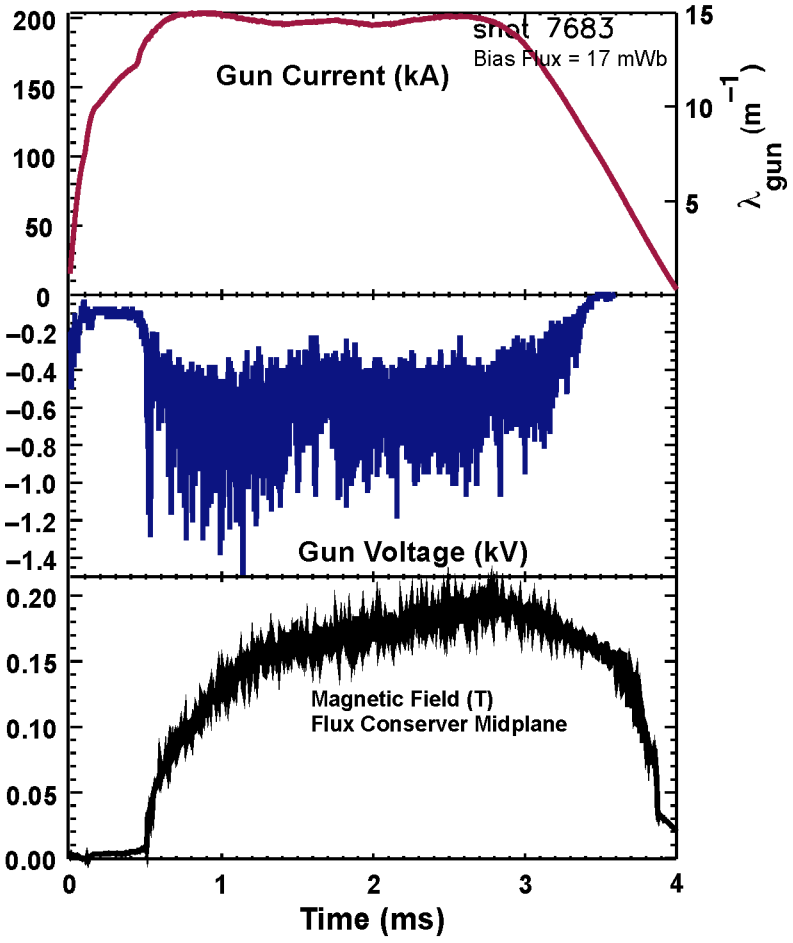
shot 7683
Bias Flux = 17 mWb
Gun Current (kA)
Gun Voltage (kV)
Magnetic Field (T)
Flux Conserver Midplane
Time (ms)
λgun (m-1)

Fig. 3

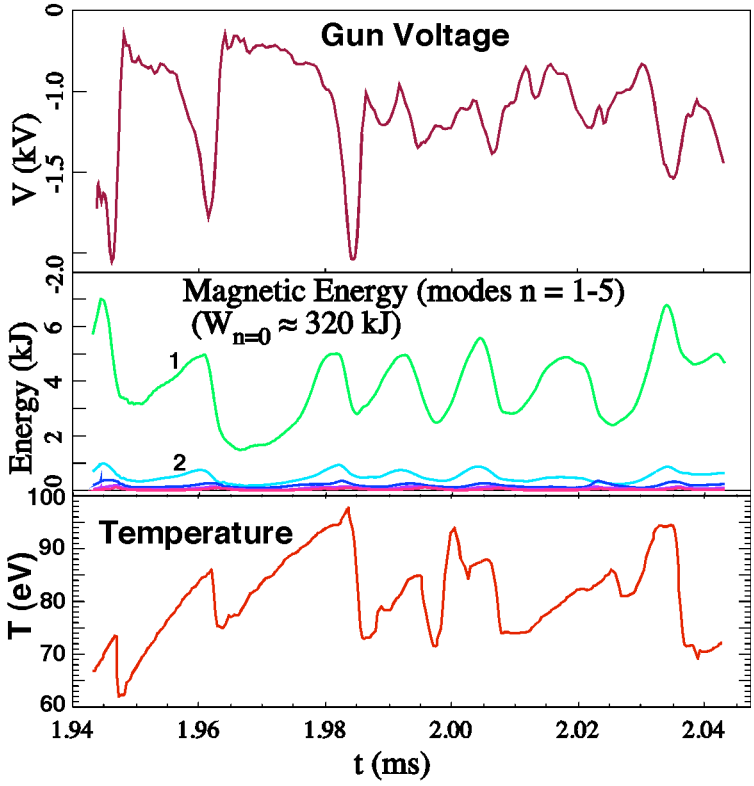
Gun Voltage
V (kV)
0
-1.0
-1.5
-2.0
Magnetic Energy (modes n = 1-5)
($W_{n=0}$ ≈ 320 kJ)
1
2
Energy (kJ)
6
4
2
0
100
Temperature
T (eV)
90
80
70
60
1.94
1.96
1.98
2.00
2.02
2.04
t (ms)

Fig. 4

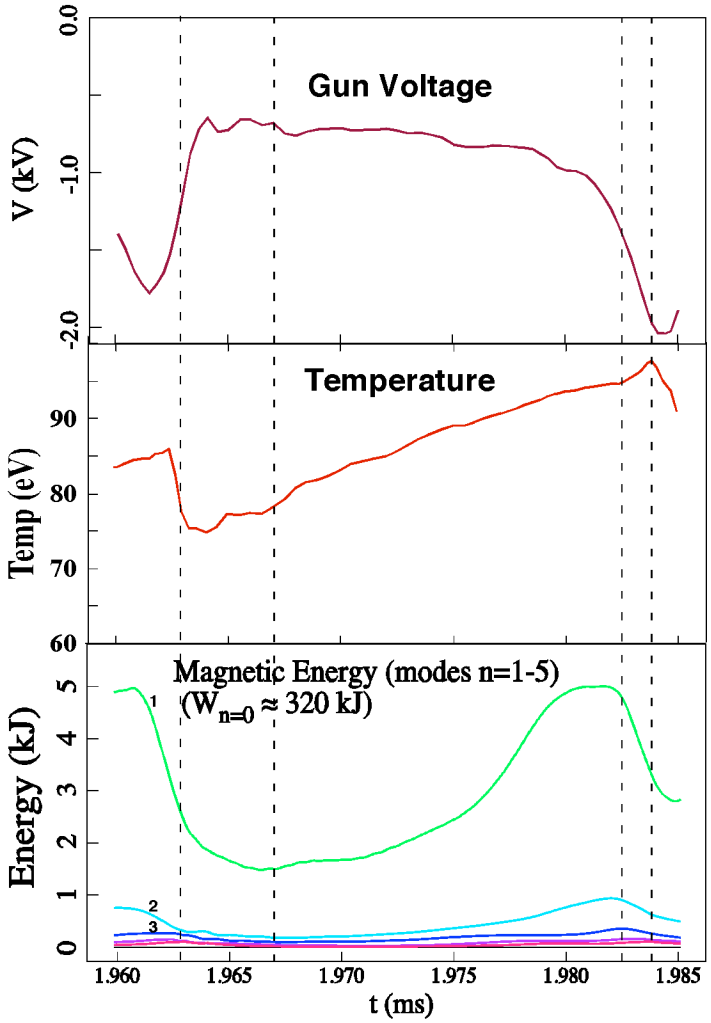
Gun Voltage
V (kV)
0.0
-1.0
-2.0
Temperature
Temp (eV)
90
80
70
60
Magnetic Energy (modes n=1-5)
($W_{n=0} \approx 320$ kJ)
Energy (kJ)
0
1
2
3
4
5
1
2
3
1.960
1.965
1.970
1.975
1.980
1.985
t (ms)

Fig. 5

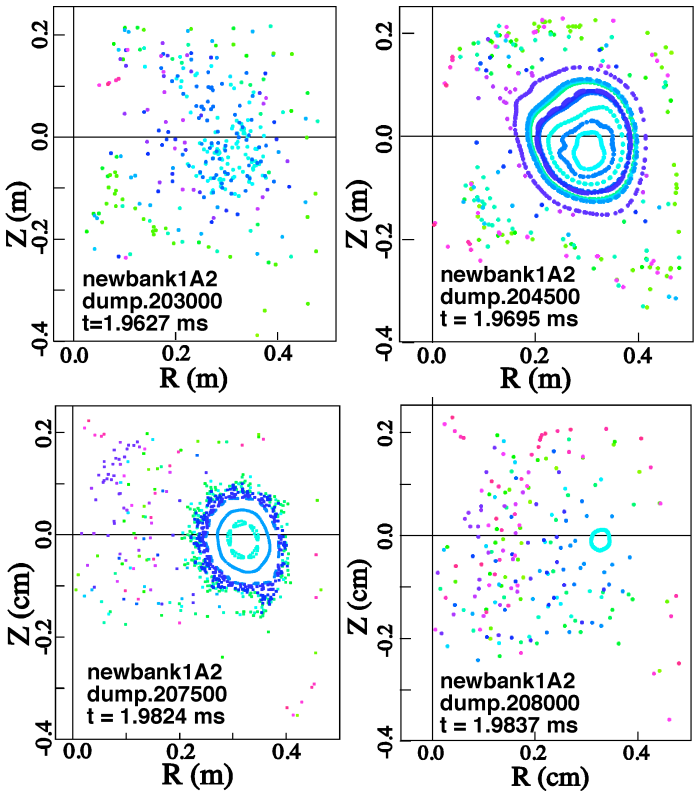
newbank1A2
dump.203000
t=1.9627 ms
newbank1A2
dump.204500
t = 1.9695 ms
newbank1A2
dump.207500
t = 1.9824 ms
newbank1A2
dump.208000
t = 1.9837 ms
Z (m)
Z (cm)
R (m)
R (cm)
0.2
0.0
-0.2
-0.4
0.0
0.2
0.4

Fig. 6

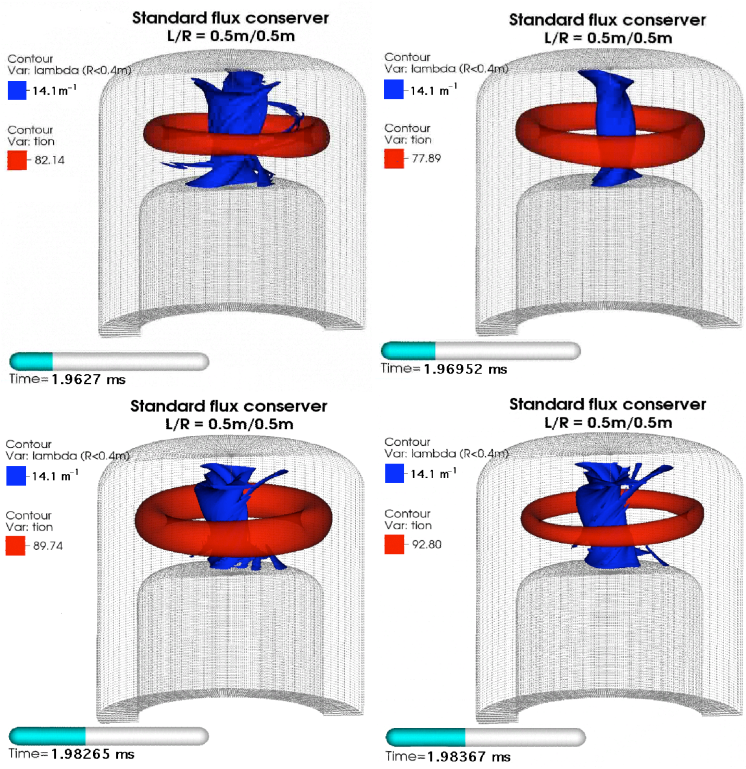
Standard flux conserver
L/R = 0.5m/0.5m
Contour
Var: lambda (R<0.4m)
14.1 m-1
Contour
Var: tion
82.14
Time= 1.9627 ms
Standard flux conserver
L/R = 0.5m/0.5m
Contour
Var: lambda (R<0.4m)
14.1 m-1
Contour
Var: tion
77.89
Time= 1.96952 ms
Standard flux conserver
L/R = 0.5m/0.5m
Contour
Var: lambda (R<0.4m)
14.1 m-1
Contour
Var: tion
89.74
Time= 1.98265 ms
Standard flux conserver
L/R = 0.5m/0.5m
Contour
Var: lambda (R<0.4m)
14.1 m-1
Contour
Var: tion
92.80
Time= 1.98367 ms

Fig. 7

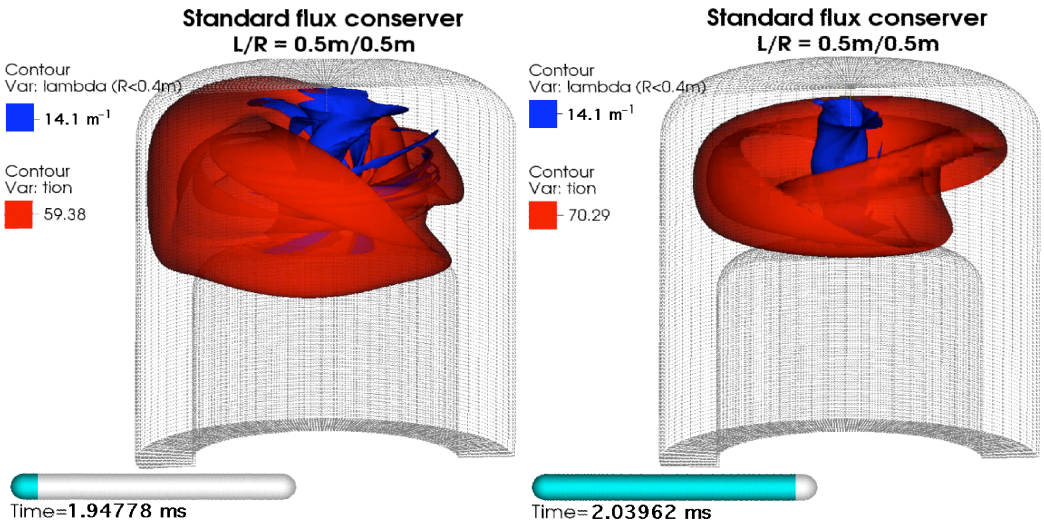
Standard flux conserver
L/R = 0.5m/0.5m
Contour
Var: lambda (R<0.4m)
14.1 m-1
Contour
Var: tion
59.38
Time=1.94778 ms
Standard flux conserver
L/R = 0.5m/0.5m
Contour
Var: lambda (R<0.4m)
14.1 m-1
Contour
Var: tion
70.29
Time=2.03962 ms

Fig. 8

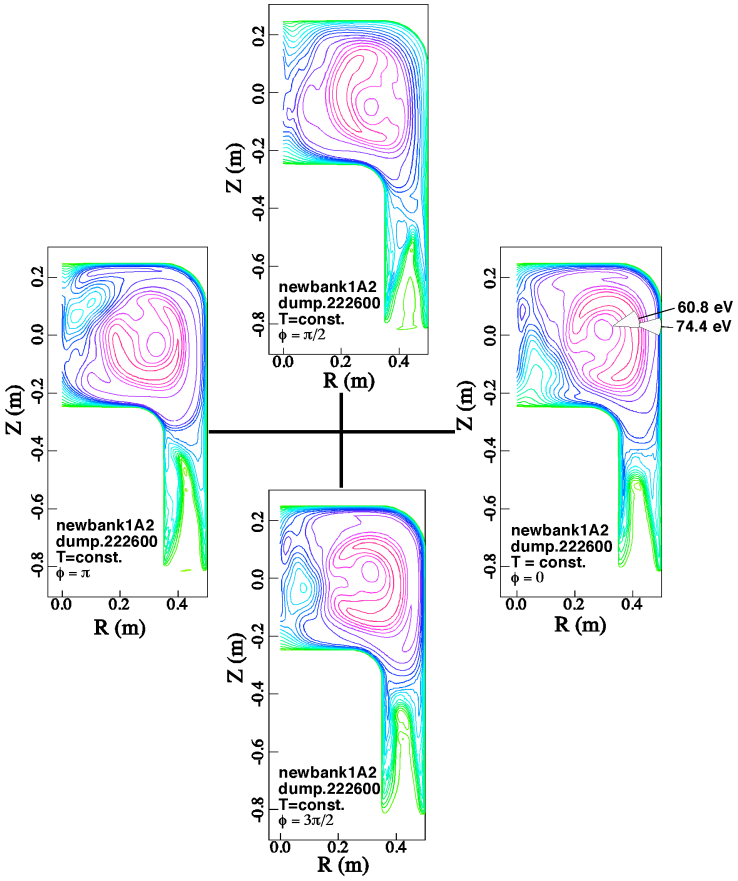
newbank1A2
dump.222600
T=const.
ϕ = π/2
newbank1A2
dump.222600
T=const.
ϕ = π
newbank1A2
dump.222600
T = const.
ϕ = 0
60.8 eV
74.4 eV
newbank1A2
dump.222600
T=const.
ϕ = 3π/2
Z (m)
R (m)

Fig. 9

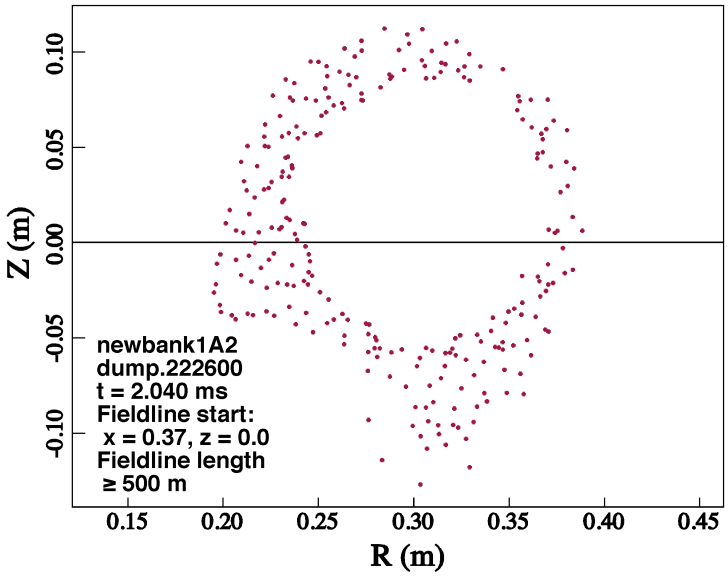
Z (m)
0.10
0.05
0.00
-0.05
-0.10
newbank1A2
dump.222600
t = 2.040 ms
Fieldline start:
x = 0.37, z = 0.0
Fieldline length
≥ 500 m
0.15
0.20
0.25
0.30
0.35
0.40
0.45
R (m)

Fig. 10

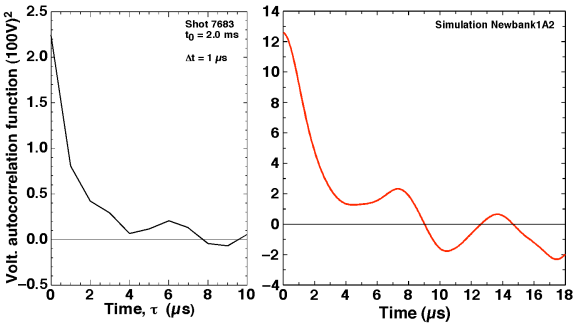
Shot 7683
t_0 = 2.0 ms
Δt = 1 μs
Volt. autocorrelation function (100V)^2
Time, τ (μs)
Simulation Newbank1A2
Time (μs)

Fig. 11

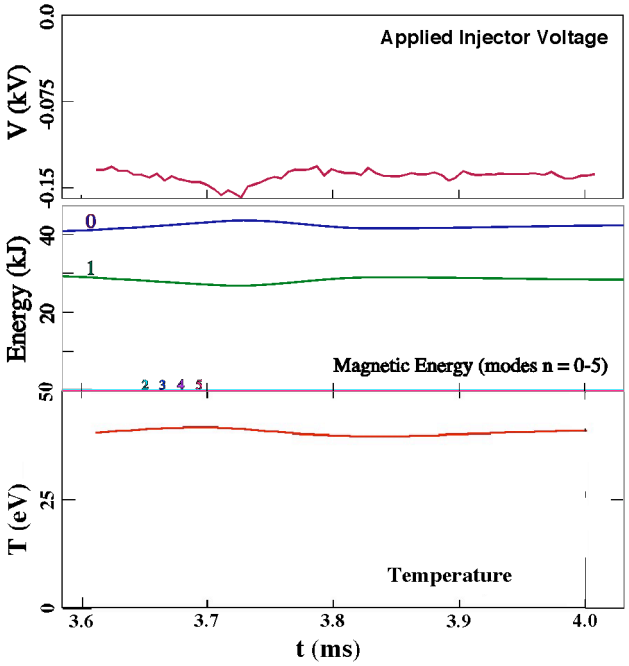
Applied Injector Voltage
V (kV)
0.0
-0.075
-0.15
0
1
Energy (kJ)
40
20
Magnetic Energy (modes n = 0-5)
2 3 4 5
50
T (eV)
25
0
Temperature
3.6
3.7
3.8
3.9
4.0
t (ms)

Fig. 12

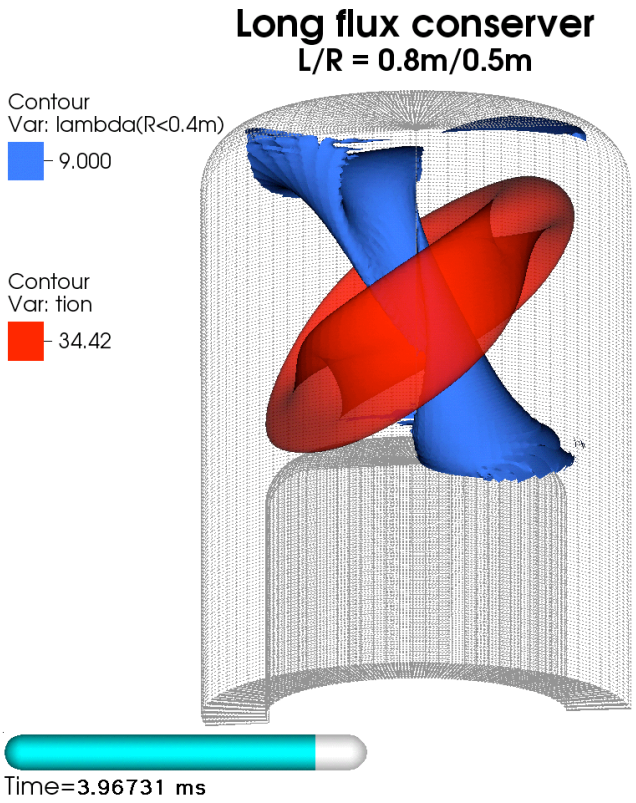
Long flux conserver
L/R = 0.8m/0.5m
Contour
Var: lambda(R<0.4m)
9.000
Contour
Var: tion
34.42
Time=3.96731 ms

Fig. 13

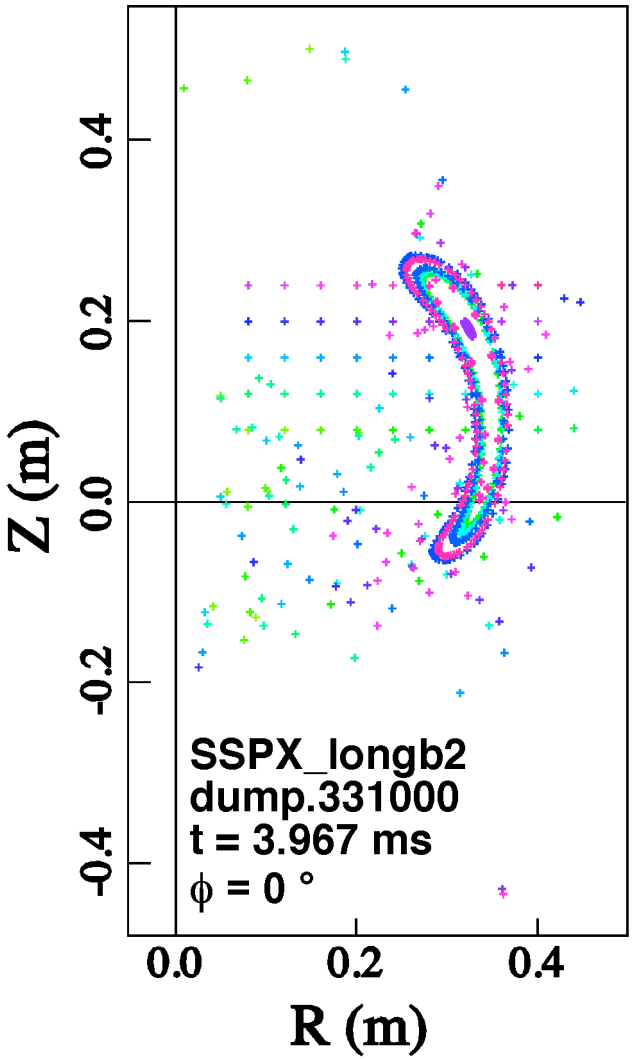

Fig. 14

30. See EPAPS Document No. .... For more information on EPAPS, see http://www.aip.org/pubservs/epaps.html.